

Journal of Electronic Imaging

JElectronicImaging.org

Exposure time calculation for spectral cameras

Ahmed Sohaib
Antonio Robles-Kelly

Exposure time calculation for spectral cameras

Ahmed Sohaib^{a,*} and Antonio Robles-Kelly^b

^aAustralian National University, Research School of Engineering, 32 North Road, Acton, ACT 2601, Australia

^bNational ICT Australia, Locked Bag 8001, Canberra, ACT 2601, Australia

Abstract. This paper presents a method for automatic exposure time adjustment for multispectral and hyperspectral cameras. The method presented here is based upon a spectral power image. Here, we use the photopic response function due to its widespread usage in photography and psychophysics. Note that, however, the method presented here is quite general in nature and can employ a number of spectral sensitivity functions for the computation of the spectral power image. Making use of this spectral power image, the exposure time is then computed via iterative updates so as to minimize the squared error between a target image and the current spectral power yielded by the imager. This target image is recovered in a straightforward manner using histogram equalization and the Commission Internationale de l'Éclairage (CIE) photopic function. This, in turn, yields an automatic method devoid of calibration targets or additional inputs. We perform a stability and controllability analysis of our method using a state-space representation. We also show the applicability of the method for exposure time calculation on staring array and multicharge coupled device architecture cameras on real-world scenes. © 2015 SPIE and IS&T [DOI: 10.1117/1.JEI.24.5.053025]

Keywords: camera auto-exposure control; state-space representations; imaging spectroscopy.

Paper 15203 received Mar. 19, 2015; accepted for publication Sep. 9, 2015; published online Oct. 13, 2015.

1 Introduction

Spectral cameras, unlike trichromatic cameras, provide information over a large number of wavelength channels across the electromagnetic spectrum. This, in effect, delivers an information-rich representation of the scene which can be used in areas such as detection,¹⁻³ classification,^{4,5} and recognition.⁶⁻⁸ Spectral imaging has also found application in areas such as color constancy⁹ and the optimal multiplexing of bandpass filtered illumination.^{10,11}

This paper proposes a method aimed at automatic exposure control for multispectral and hyperspectral cameras. Note that due to the complex nature of these imagers, exposure control techniques that pertain to trichromatic cameras are not applicable in a straightforward manner to imaging spectroscopy.¹² Further, automatic exposure control is a desirable feature in settings where the image acquisition is done in environments when the illumination is prone to change, delivering images with a consistent, reproducible distribution of brightness values. It is also desired since the dynamic range (the ratio between the maximum and minimum intensity values) of many real-world scenes far exceeds that of many cameras. As a result, an incorrect exposure setting yields dark or overexposed imagery with a reduced contrast.

A significant amount of research has been undertaken for trichromatic camera exposure control. However, very little work has been done in the domain of multispectral and hyperspectral cameras. Work done for trichromatic cameras is mostly in the form of commercial patents (US patent classification class number 354 and subclass 410 to 455). Early techniques often rely upon external hardware for light metering.¹³ Later on, through-the-lens (TTL) brought the metering

setup inside the digital camera.¹⁴ Nonetheless, TTL metering techniques were widely employed in camcorders, but their main drawback stemmed from their computational complexity.

Subsequently, photometric sensors have steadily replaced TTL systems for exposure control.¹⁵ These employ the brightness information to estimate the exposure control parameters. For instance, Kuno et al.¹⁵ use the brightness value of a charge coupled device (CCD) sensor and an iterative lookup-table-method to decrease the amount of time taken to compute the exposure value as compared to a TTL system. Liang et al.¹⁶ have improved Kuno's technique by introducing iterative updates based on predefined lookup tables. Similarly, Bell et al.¹⁷ use an initial image histogram and compare its mean against a predefined value. Shimizu et al.¹⁸ have used a different criterion named HIST, which employs the brightness ratio for the pixels in the image to adjust the exposure time.

Most modern automatic exposure algorithms use scene analysis techniques such as spot, matrix, evaluative, and center-weighted metering to analyze the brightness of a scene or an object of interest and to adjust the exposure setting accordingly. To compensate for back lit scenes, Lee et al.¹⁹ propose a division of the image into several areas assuming that the main object of interest tends to be in the center of the scene. Nourani-Vatani and Roberts²⁰ present a method where various masks are applied so as to obtain the exposure adjustment using the settings for the lens, environment, and the area of interest. Similarly, Rogers and Cope²¹ use human flesh regions in the scene to control the exposure of the camera. His work is particularly well suited to improve the appearance of the human subjects in portraits and snapshots acquired by hand-held devices.

*Address all correspondence to: Ahmed Sohaib, E-mail: ahmed.sohaib@nicta.com.au

For exposure control of spectral cameras, calibration targets are often used to adjust the exposure. A model for such calibration is presented in the work of Brelstaff et al.²² Unfortunately, photometric exposure calibration with a white reference target is infeasible or impractical in many real-world settings. In Ref. 23, the authors develop an automatic exposure approach which does not require a calibration target.

Here, we compute the exposure time based upon a formal stability analysis which assures controllability conditions are satisfied. This, in turn, yields a method which can be applied to a broad range of cameras with varying architectures and acquisition schemes. Moreover, in order to improve the stability of the method presented here, an error image is used for the exposure time estimation. This error image is, hence, the difference between the target image and the spectral power image of the current scene, as yielded by the Commission Internationale de l'Éclairage (CIE) 1931 photopic function. Thus, the method presented here has a number of advantages with respect to that in Ref. 23. First, its controllability is assured. Second, the error image used here is an additional constraint as compared to the target image employed in Ref. 23. Finally, the use of control theory and the error image allows for the introduction of a regularization term in our cost function. This, in effect, implies that the optimization problem solved here is different from that in Ref. 23.

The paper is organized as follows. In Sec. 2, we commence by presenting the theoretical background used throughout the paper. In Sec. 3, we develop our method for automatically estimating the exposure time. In Sec. 4, we present our stability analysis for the state-space representation of the method and elaborate on its controllability conditions. In Sec. 5, we show the applicability of our method for setting the exposure of a multiple-CCD multispectral camera and a staring arrays hyperspectral camera. In our experiments, we used a Macbeth ColorChecker to validate the quality of the results. Finally, in Sec. 6, we conclude on the research presented throughout.

2 Background

A CCD is a device that converts the photons from a scene into a digital count. The ratio of the incoming photons to the number of photoelectrons produced is called the “quantum efficiency.” In CCDs, these photoelectrons are converted into a numerical value, usually referred to as “data number” or simply “count.” The “gain” of the CCD is defined as the conversion factor between the produced electrons and the count. Note that if we allow more photons to reach the CCD by gradually increasing the exposure, the mean count of the CCD will increase accordingly. Hence, there is a strong correlation between exposure value and image quality.

Theoretically, if the shutter is closed and we capture an image with a short exposure time, there should not be any photons arriving at the CCD. However, in practice, the count is not null. This is due to the presence of dark current and CCD bias. Dark current is the small electric current flowing through the CCD when theoretically no photons are entering the camera. Dark current is dependent on the temperature of the CCD, where a high CCD temperature will result in higher dark current values. Bias often appears

as a regular pattern on the image which arises from the pixel-to-pixel variations of the offset level on the CCD count. The dark current and bias should be subtracted from the image in order to properly estimate the photons and their conversion. Using the quantum efficiency, dark current, and bias, we can express the data number as

$$O_{\text{DN}} = \frac{1}{g}(FQT + \psi T + \beta), \quad (1)$$

where O_{DN} is the observed data number, g is the gain, F is the photon flux impinging on the CCD, Q is the quantum efficiency, T is the exposure time, ψ is the dark current, and β is the bias.

Note that due to the broader dynamic range of spectral imagers as compared to traditional trichromatic cameras, here we assume that the CCD response is linear. To remove the effect of dark current and bias, the common practice is to take an image with a closed shutter, such that the photon flux becomes zero, i.e., $FQT \rightarrow 0$. The new equation becomes

$$O' = \frac{1}{g}(\psi T + \beta). \quad (2)$$

If we subtract O' from O_{DN} our observed data number will be

$$O = \frac{1}{g}(FQT). \quad (3)$$

The importance of the expression above resides in the fact that it implies that the effects of dark current and bias can be safely ignored and removed automatically at start-up or with a periodic dark current acquisition routine.

Consider the multispectral image I whose pixels are indexed to the row and column coordinates and the wavelength index λ . In some cameras, every wavelength channel has an associated exposure time. This is often the case with staring array systems such as the opto-knowledge systems, incorporation (OKSI) hyperspectral cameras. Other systems use a single exposure time for multiple wavelength-indexed bands. This is the case for multiple-CCD systems such as the FluxData multispectral cameras. In the case of the FluxData camera, seven wavelength channels are acquired from three CCDs. Each CCD has its own exposure setting. For the sake of generality, we assume that m wavelength channels are divided into c sets, where each wavelength set Λ_j has its own exposure time T_j for $j = 1, 2, \dots, c$. For cameras where every wavelength has its own exposure time (e.g., the OKSI systems), c is equal to m . Let us assume that the pixel values we get from a camera are actual “data numbers.” We can then rewrite Eq. (3) as

$$I(v, \lambda) = F(v, \lambda)Q(\lambda)T_j, \quad (4)$$

where $j = 1, \dots, c$, which relates to the wavelength sets. $I(v, \lambda)$ is the pixel value at location v and channel λ . $F(v, \lambda)$ is the photon flux impinging on pixel v , $Q(\lambda)$ is the quantum efficiency for the channel corresponding to the wavelength λ , and T_j is the exposure time for the wavelength set Λ_j . It is also worth noting in passing that the gain g is a constant that has been absorbed into the equation above.

Further, we can write

$$F(v, \lambda)Q(\lambda) = \mathcal{V}(v, \lambda), \quad (5)$$

where $\lambda \in \Lambda_j$. Note that $\mathcal{V}(v, \lambda)$ is referred to as the irradiance on the sensor at pixel location v , which can be calculated using Eq. (4).

3 Exposure Time Recovery

Following the equation above, we can estimate the exposure time by comparing the image yielded by the current exposure time setting with respect to an “ideal” target image. Also, recall that the luminous flux of light sources is based upon the CIE photopic function.²⁴ This function is a smooth one across the spectral domain, hence here we also adopt the notion that the exposure times should not change steeply across adjacent wavelength-indexed bands. At the same time, we also require the method to be stable, assuring convergence. In the following section, we present our method to estimate the exposure time. We also present a controllability analysis.

3.1 Optimization

Considering Eqs. (4) and (5), the initial image acquired from the spectral camera can be written as

$$I(v, \lambda) = \mathcal{V}(v, \lambda)T_j. \quad (6)$$

Note that spectral images can be viewed as “cubes,” where the x - and y -axes represent the spatial coordinates, and the z -axis represents the spectral domain. Having the initial image cube in hand, we can generate a target image from which subsequent updates can be computed via an optimization approach. To this end, we employ a spectral power image, which is computed making use of the CIE photopic function²⁴ so as to weight the contribution of each spectral band to the power at each pixel. This yields

$$\hat{I}(v) = \sum_{j=1}^c \sum_{\lambda \in \Lambda_j} \mathcal{V}(v, \lambda)W(\lambda)T_j, \quad (7)$$

where $W(\lambda)$ represents the photopic function at channel λ . Note that our method is quite general in nature, allowing for other spectral sensitivity functions to be applied instead. Here, we have used the photopic function due to both its widespread use in photography and its relation to the response of the human eye in well-lit environments.²⁵ Similarly, in low-light conditions, a scotopic function can be used. Other choice of functions can be made based on the application domain.

It can be observed that the spectral power image $\hat{I}(v)$ is obtained by adding the weighted response for each channel. For simplicity, we can write

$$Y(v, \lambda) = \mathcal{V}(v, \lambda)W(\lambda), \quad (8)$$

such that $\hat{I}(v)$ becomes

$$\hat{I}(v) = \sum_{j=1}^c \sum_{\lambda \in \Lambda_j} Y(v, \lambda)T_j. \quad (9)$$

Assuming N pixels in a single channel, Eq. (9) can be rewritten in matrix form as follows:

$$\hat{I} = \mathbf{X}T, \quad (10)$$

where $\hat{I} = [\hat{I}(1), \hat{I}(2), \dots, \hat{I}(N)]^T$ and $T = [T_1, T_2, \dots, T_c]^T$ are the vectors and \mathbf{X} is a matrix defined as

$$\mathbf{X} = [y_1, y_2, \dots, y_m][\mathbf{1}_{\Lambda_1}, \mathbf{1}_{\Lambda_2}, \dots, \mathbf{1}_{\Lambda_c}], \quad (11)$$

where $y_i = [Y(1, \lambda_i), Y(2, \lambda_i), \dots, Y(N, \lambda_i)]^T$ for $i = 1, 2, \dots, m$. $\mathbf{1}_{\Lambda_j}$ is an indicator function which results in a binary column vector of length m such that Λ_j is a subset of $[\lambda_1, \lambda_2, \dots, \lambda_m]^T$ and $\mathbf{1}_{\Lambda_j}(\lambda_i) = 1$ if $\lambda_i \in \Lambda_j$, and 0 otherwise. Thus, \mathbf{X} captures the combined effect of the irradiance by making use of the photopic response per exposure time for each wavelength set Λ_j .

In order to obtain a target image for our optimization strategy, we use histogram equalization as applied to the spectral power image \hat{I} . Our choice of histogram equalization stems from the fact that this effectively “stretches” the input image intensities across the dynamic range uniformly resulting in a better contrasted image. It should also be noted, however, that histogram equalization produces unrealistic results for the cases when the dynamic range of the scene is significantly low. It is also worth noting in passing that the histogram-equalized image serves as a reference for our method, hence other approaches can be used as dictated by the application or lighting conditions.

Our histogram-equalized image hence becomes

$$\mathcal{I} = \text{histeq}(\hat{I}), \quad (12)$$

where $\text{histeq}(\cdot)$ is the image equalization operator of choice.

To estimate the update in the exposure time, we employ the difference between the input and the target image given by

$$e[k] = \mathcal{I} - \hat{I}[k], \quad (13)$$

where $e[k]$ and $\hat{I}[k]$ are the error and spectral power images at iteration k , respectively. Note that, in the equation above and throughout the paper, we opt to use the notation commonly found in time series analysis for the iteration indexing of the variables. We have done this for the sake of consistency with respect to the common treatment of state-space analysis in the control literature.

Note that, since the input images are all of the same scene, we can consider the target equalized images to be invariant. In practice, these may also be indexed to iteration number in a straightforward manner. For the sake of simplicity, we consider the ideal case and treat \mathcal{I} as being devoid of k . Also, it is worth noting in passing that in many modern cameras, metering methods like centered, spot, or matrix metering are used. These methods apply various weighting techniques to different parts of the scenes, which can be incorporated effortlessly by the introduction of a per-pixel prior on the difference equation above.

From Eq. (10), it can be observed that the image values are related to their exposure time as set in the matrix \mathbf{X} . As a result, we can use Eq. (13) to relate the change in the exposure time to the error at iteration k as follows:

$$e[k] = \mathbf{X}\Delta[k], \quad (14)$$

where $\Delta[k]$ is the update in the exposure time. Thus, the updated exposure time can be calculated using the rule

$$T[k+1] = T[k] + \alpha\Delta[k], \quad (15)$$

where α is the update step size, which suggests the magnitude of change. Note that the larger the value of α , the steeper will be the change in the exposure time.

Note that the exposure times are related to the camera architecture through the wavelength sets in each Λ_j . This is because these wavelengths correspond to each of the exposure times T_j , which, in turn, depend on the imager. Thus, here, we employ a cost function which aims at both, minimizing the error $\epsilon[k]$, but also penalizing exposure times which are far removed from the average across the imager, i.e., we regularize T_j across all the wavelength sets. Our cost function is thus defined as

$$J(\mathcal{T}) = \epsilon^2[k] + \eta \sum_{j=1}^c [\gamma - T_j]^2, \quad (16)$$

where T_j is the balanced exposure time for wavelength set Λ_j which needs to be estimated, γ is the average of exposure times such that $\gamma = 1/c \sum_{j=1}^c T_j$, where $[T_1, T_2, \dots, T_c]^T = T[k+1]$ which is estimated in Eq. (15). η is a scalar that controls the contribution of the second term of the minimization in hand. Using Eqs. (10) and (13), the cost function can be represented in matrix form as follows:

$$J(\mathcal{T}) = (\mathcal{I} - \mathbf{X}\mathcal{T})^T (\mathcal{I} - \mathbf{X}\mathcal{T}) + [\sqrt{\eta}(\Gamma - \mathcal{T})]^T [\sqrt{\eta}(\Gamma - \mathcal{T})]. \quad (17)$$

Here, each column of \mathbf{X} represents a wavelength-indexed channel multiplied by its photopic function value and Γ is a column vector whose entries are given by γ . As a result, Eq. (17) can be simplified and rewritten as

$$J(\mathcal{T}) = \left[\begin{array}{c} \mathcal{I} - \mathbf{X}\mathcal{T} \\ \sqrt{\eta}\Gamma - \sqrt{\eta}\mathcal{T} \end{array} \right]^T \left[\begin{array}{c} \mathcal{I} - \mathbf{X}\mathcal{T} \\ \sqrt{\eta}\Gamma - \sqrt{\eta}\mathcal{T} \end{array} \right], \quad (18)$$

which yields the minimization

$$\min_{\mathcal{T}} \left\| \left[\begin{array}{c} \mathcal{I} \\ \sqrt{\eta}\Gamma \end{array} \right] - \left[\begin{array}{c} \mathbf{X} \\ \sqrt{\eta}\mathbf{I} \end{array} \right] \mathcal{T} \right\|^2, \quad (19)$$

s.t. $\mathcal{T} \geq 0$

where \mathbf{I} represents the identity matrix and, since the exposure times cannot be negative, we have explicitly imposed a non-negativity constraint.

The stopping criterion for our iterative updates is governed by the normalized error given by

$$\hat{\epsilon}[k] = \frac{|\epsilon[k]|}{|\mathcal{I}|}. \quad (20)$$

Thus, if $\hat{\epsilon}[k]$ is smaller than a predefined threshold, we can conclude that convergence has been reached. This is in accordance with the notion that if the exposure times are optimum, the difference between the spectral power image and the histogram-equalized scene is expected to be nil.

4 Stability Analysis

Our objective as presented above is to update the exposure time such that the spectral power image is in good accordance with the histogram-equalized reference. In order to

ensure that the presented method is, indeed, stable, i.e., that our approach will yield exposure time updates to convergence, here we present a stability analysis based upon state space. This also allows for the determination of the conditions upon which our approach is to remain controllable, i.e., will not diverge. Thus, in this section, we commence by transforming the equations above into their state space form²⁶ and then apply the stability and controllability criteria using concepts from control theory.

4.1 State-Space Representation

State-space representations are widely used in control theory in order to analyze systems with multiple inputs and outputs by making use of state variables. Recall that the general form of a state-space representation is given by the equations:

$$\mathbf{x}[k+1] = \mathbf{A}\mathbf{x}[k] + \mathbf{B}\mathbf{u}[k], \quad (21)$$

$$\mathbf{y}[k] = \mathbf{C}\mathbf{x}[k] + \mathbf{D}\mathbf{u}[k]. \quad (22)$$

Equation (21) is often called the state equation whereas Eq. (22) is referred to as the output equation. In the above expressions, \mathbf{x} is a vector containing the state variables, \mathbf{u} is the input vector, \mathbf{A} is the transition matrix between state variables, the matrix \mathbf{B} captures the relationship between input and state variables, the matrix \mathbf{C} relates to the state variables with the outputs, and \mathbf{D} is the transfer matrix between the input variables and the output.

For our approach, Eqs. (13) and (15) are those required for the state-space representation. To this end, we can write

$$\left[\begin{array}{c} \hat{\mathcal{I}}[k+1] \\ T[k+1] \end{array} \right] = \left[\begin{array}{cc} \mathbf{0} & \mathbf{0} \\ \mathbf{0} & \mathbf{I} \end{array} \right] \left[\begin{array}{c} \hat{\mathcal{I}}[k] \\ T[k] \end{array} \right] + \left[\begin{array}{cc} \mathbf{I} & \mathbf{0} \\ \mathbf{0} & \mathbf{R} \end{array} \right] \left[\begin{array}{c} \mathcal{I} \\ \epsilon[k] \end{array} \right], \quad (23)$$

where $\mathbf{0}$ is a matrix whose entries are all zero, \mathbf{I} is the identity matrix, and $\mathbf{R} = (\mathbf{X}^T\mathbf{X})^{-1}\mathbf{X}^T$.

The output equation is given by

$$\mathbf{y}[k] = [\mathbf{0} \quad \mathbf{I}] \left[\begin{array}{c} \hat{\mathcal{I}}[k] \\ T[k] \end{array} \right]. \quad (24)$$

We assume we have r inputs, s states, and q outputs. From the above equations, it can be observed that $r = |\mathcal{I}| + |\epsilon[k]|$, $s = |\hat{\mathcal{I}}| + c$, and $q = c$, where $|\cdot|$ yields the number of elements in the array or vector under consideration. Note that if p number of pixels are used instead of a complete image then $r = p + p$. For the reference of the reader, in Table 1, we summarize the variables in the state space and output equations with their respective value and dimensionality.

4.2 Stability Analysis of the Method

In control theory, a system can be either stable or not based upon its output. In state-space representations, the stability of a system is determined by analyzing the eigenvalues of the matrix \mathbf{A} . As mentioned earlier, the matrix \mathbf{A} determines the relationship between the current state variables and those at the next iteration. A discrete time system will be unstable if any of the eigenvalues of matrix \mathbf{A} has a magnitude greater than unity. On the other hand, a discrete time system will be stable if all the eigenvalues of matrix \mathbf{A} have magnitudes less than 1. For a marginally stable system, the eigenvalue magnitudes are equal to 1. Those eigenvalues, whose magnitudes

Table 1 Equivalence between the variables in the state-space equations and those used in Sec. 3.1. Here, we have $r = |\mathcal{I}| + |e[k]|$, $s = |\hat{I}| + c$, and $q = c$, where $|\cdot|$ yields the number of elements in the array or vector under consideration.

Equation variables	Description	Dimensionality	Values
\mathbf{x}	Vector of state variables	$s \times 1$	$\begin{bmatrix} \hat{I}[k] \\ T[k] \end{bmatrix}$
\mathbf{u}	Vector of input values	$r \times 1$	$\begin{bmatrix} \mathcal{I} \\ e[k] \end{bmatrix}$
\mathbf{A}	Transition matrix between state variables	$s \times s$	$\begin{bmatrix} \mathbf{0} & \mathbf{0} \\ \mathbf{0} & \mathbf{I} \end{bmatrix}$
\mathbf{B}	Relationship matrix between input and state variables	$s \times r$	$\begin{bmatrix} \mathbf{I} & \mathbf{I} \\ \mathbf{0} & \mathbf{R} \end{bmatrix}$
\mathbf{C}	Relationship matrix between state variables and output	$q \times s$	$[\mathbf{0} \ \mathbf{I}]$
\mathbf{D}	Transfer matrix between input and output	$q \times r$	$[\mathbf{0} \ \mathbf{0}]$

are unity, must also be simple roots of the characteristic polynomial of \mathbf{A} . In other words, the Jordan blocks of matrix \mathbf{A} must be of first order.²⁶

From Table 1, it becomes evident that the eigenvalues of matrix \mathbf{A} are either 0 or 1. It can also be observed that unity eigenvalues correspond to the simple root of the characteristic polynomial of \mathbf{A} . Furthermore, it can be shown that the number of nil eigenvalues relates to the number of pixels in \hat{I} , whereas the number of unity eigenvalues is determined by the number of exposure times used by the system.

Thus, if, for instance, the system is a multiple-CCD one, the number of unity eigenvalues is equal to the number of CCDs. If the system exposure time is channel-based, i.e., one exposure time per wavelength-indexed band, then the number of unity eigenvalues equals the number of bands in the image. Further, these unity eigenvalues suggest that our method is marginally stable (the state of the system will converge with “oscillations” to the optimal exposure time when the iteration number tends to infinity). Note that this is not a problem in practice due to the use of the stopping criterion presented earlier. This is because the threshold allows for the method to stop even when these oscillations may be present in its asymptotic behavior.

4.3 Controllability of the Method

Another important aspect of the system which is worth exploring is the controllability of the method. Controllability helps to determine the effect of the inputs on the system. A state is controllable at iteration k if there exists an input that delivers the desired output as $k \rightarrow \infty$.

In order to determine the controllability of the system, a controllability matrix \mathbf{P} is usually constructed using the matrix \mathbf{A} and the input matrix \mathbf{B} . The matrix \mathbf{P} is given by

$$\mathbf{P} = [\mathbf{B} \ \mathbf{AB} \ \mathbf{A}^2\mathbf{B} \ \dots \ \mathbf{A}^{s-1}\mathbf{B}], \quad (25)$$

where the dimension of $\mathbf{P} = s \times rs$.

For all the states to be controllable, matrix \mathbf{P} is required to be full row rank. This refers to the case whereby all the states will converge to the desired state asymptotically. If the matrix \mathbf{P} is found to be rank deficient, then such states need to be separated from the rest and analyzed in order to determine those inputs which render them uncontrollable.

The matrix \mathbf{P} can be found by first estimating the state-space matrix products, \mathbf{AB} , $\mathbf{A}^2\mathbf{B}$, ..., $\mathbf{A}^{s-1}\mathbf{B}$. For our method, these are given by

$$\begin{aligned} \mathbf{AB} &= \begin{bmatrix} \mathbf{0} & \mathbf{0} \\ \mathbf{0} & \mathbf{I} \end{bmatrix} \begin{bmatrix} \mathbf{I} & \mathbf{I} \\ \mathbf{0} & \mathbf{R} \end{bmatrix} = \begin{bmatrix} \mathbf{0} & \mathbf{0} \\ \mathbf{0} & \mathbf{R} \end{bmatrix} \\ \mathbf{A}^2\mathbf{B} &= \mathbf{A}(\mathbf{AB}) \\ &= \begin{bmatrix} \mathbf{0} & \mathbf{0} \\ \mathbf{0} & \mathbf{I} \end{bmatrix} \begin{bmatrix} \mathbf{0} & \mathbf{0} \\ \mathbf{0} & \mathbf{R} \end{bmatrix} = \begin{bmatrix} \mathbf{0} & \mathbf{0} \\ \mathbf{0} & \mathbf{R} \end{bmatrix} \\ &\vdots \\ \mathbf{A}^{s-1}\mathbf{B} &= \mathbf{A}(\mathbf{A}^{s-2}\mathbf{B}) \\ &= \begin{bmatrix} \mathbf{0} & \mathbf{0} \\ \mathbf{0} & \mathbf{I} \end{bmatrix} \begin{bmatrix} \mathbf{0} & \mathbf{0} \\ \mathbf{0} & \mathbf{R} \end{bmatrix} = \begin{bmatrix} \mathbf{0} & \mathbf{0} \\ \mathbf{0} & \mathbf{R} \end{bmatrix}. \end{aligned}$$

Using the matrices above, the controllability matrix \mathbf{P} becomes

Algorithm 1 Estimate exposure time.

```

1: Procedure Exposure( $T_i$ )
2:   Initialize the exposure time when  $k = 1$ ,  $T[k] \leftarrow T_i$ 
3:   for  $k = 1, \dots, \text{maxIterations}$  do
4:     Acquire cube image  $I(v, \lambda)$ 
5:     Generate spectral power image using photopic function in
       Eq. (7)  $\hat{I}(v) \leftarrow I(v, \lambda)$ 
6:     Generate target image using histogram equalization in
       Eq. (12):  $\mathcal{I} \leftarrow \hat{I}$ 
7:     Compute  $\Delta[k]$  using Eq. (14)
8:     Find  $T[k + 1]$  using  $\Delta[k]$  using Eq. (15)
9:     Balance  $T[k + 1]$  using cost function in Eq. (19):
        $T[k + 1] \leftarrow \mathcal{I}$ 
10:    Find normalized error  $\hat{e}$  using Eq. (20)
11:    if  $\hat{e} \leq \text{threshold}$  then
12:      break for
13:    end if
14:  end for
15:  Return  $T_{\text{final}} \leftarrow T[k + 1]$ 
16: end procedure

```

$$P = \begin{bmatrix} \mathbf{I} & \mathbf{I} & | & \mathbf{0} & \mathbf{0} & | & \dots & | & \mathbf{0} & \mathbf{0} \\ \mathbf{0} & \mathbf{R} & | & \mathbf{0} & \mathbf{R} & | & \dots & | & \mathbf{0} & \mathbf{R} \end{bmatrix}. \quad (26)$$

Note that the matrix \mathbf{P} depends on the matrix \mathbf{R} in terms of its row rank. Since $\mathbf{R} = (\mathbf{X}^T \mathbf{X})^{-1} \mathbf{X}^T$, it can be observed that \mathbf{R} is derived from \mathbf{X} , which contains the irradiance weighted by the photopic response for each exposure time. Moreover, for p pixels and c channels, \mathbf{X} has dimensions $p \times c$ and \mathbf{R} has a dimensionality of $c \times p$. Thus, in order for our method to remain controllable, the matrix \mathbf{R} should be full rank. As a result, our method requires at least c linearly

independent pixels over the whole range of wavelength-indexed bands for Eqs. (13) and (15) to remain controllable. This is due to the fact that using at least c linearly independent pixels across the c channels under consideration implies the matrix \mathbf{R} has c linearly independent rows. This also assures the column rank of \mathbf{P} is at least $c + p$, which, in turn, satisfies the controllability condition for our method.

Hence, typical uncontrollable cases would be those in which, for instance, a single pixel is used. Recall that, for a single pixel, \mathbf{X} becomes a vector and, as a result, \mathbf{P} becomes row rank deficient. Other cases are those where the matrix \mathbf{P}

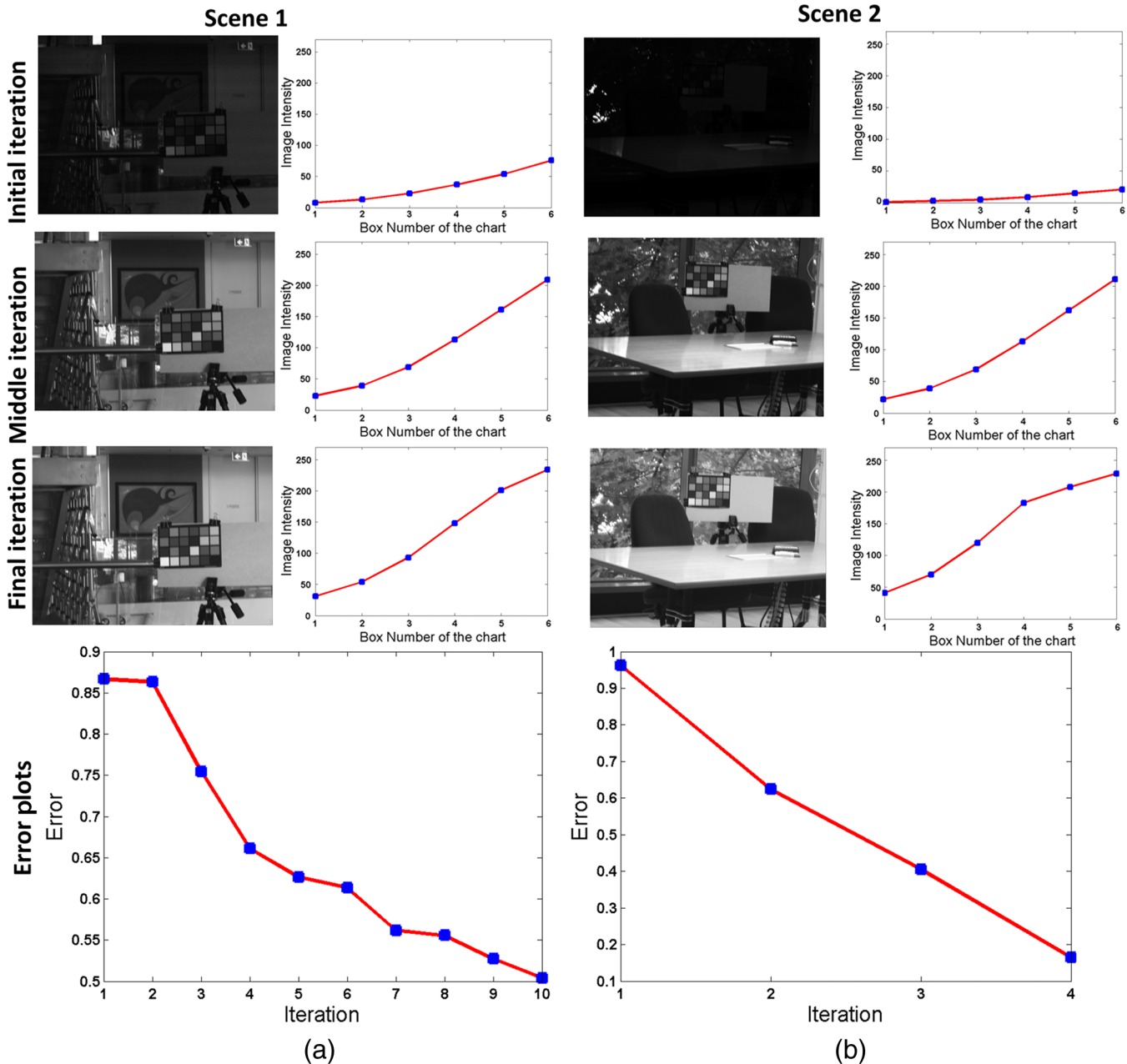


Fig. 1 FluxData multispectral camera scenes. (a) Spectral power image and (b) color chart gray-tile intensity plots (the x-axis corresponds to the index of the tile and the y-axis to the photopic response). In this figure, the top row shows the initial images, whereas the second row corresponds to the images produced by the exposure times at the iteration corresponding to the middle point over the convergence of our method. The third row shows the image acquired using the exposure time yielded by our method after convergence has been reached. Finally, the bottom row shows the normalized error plots as a function of iteration number.

is row rank deficient due to linear dependency between the pixels. This is the case, for instance, when every channel or CCD captures a completely dark image, which corresponds to $\mathbf{X} \equiv 0$, and thus every row of \mathbf{R} is also nil.

5 Results and Discussion

In Algorithm 1, we show the step sequence for our algorithm. Note that the algorithm departs from an initial exposure time and iterates until convergence is reached (the normalized error is below a predefined threshold). Moreover, it is worth

noting in passing that, in practice, these iterations are not overly computationally intensive. This is because the problem is essentially a constrained least squares optimization one, which has been thoroughly studied in the numerical methods literature.²⁷ For step 6, we have applied the histogram equalization method of Bassiou and Kotropoulos²⁸ with a uniform target histogram. We would like to stress that the choice of method to compute the reference image in step 6 or the equalization technique is not prohibitive and other methods elsewhere in the literature may also be used without any loss of generality.

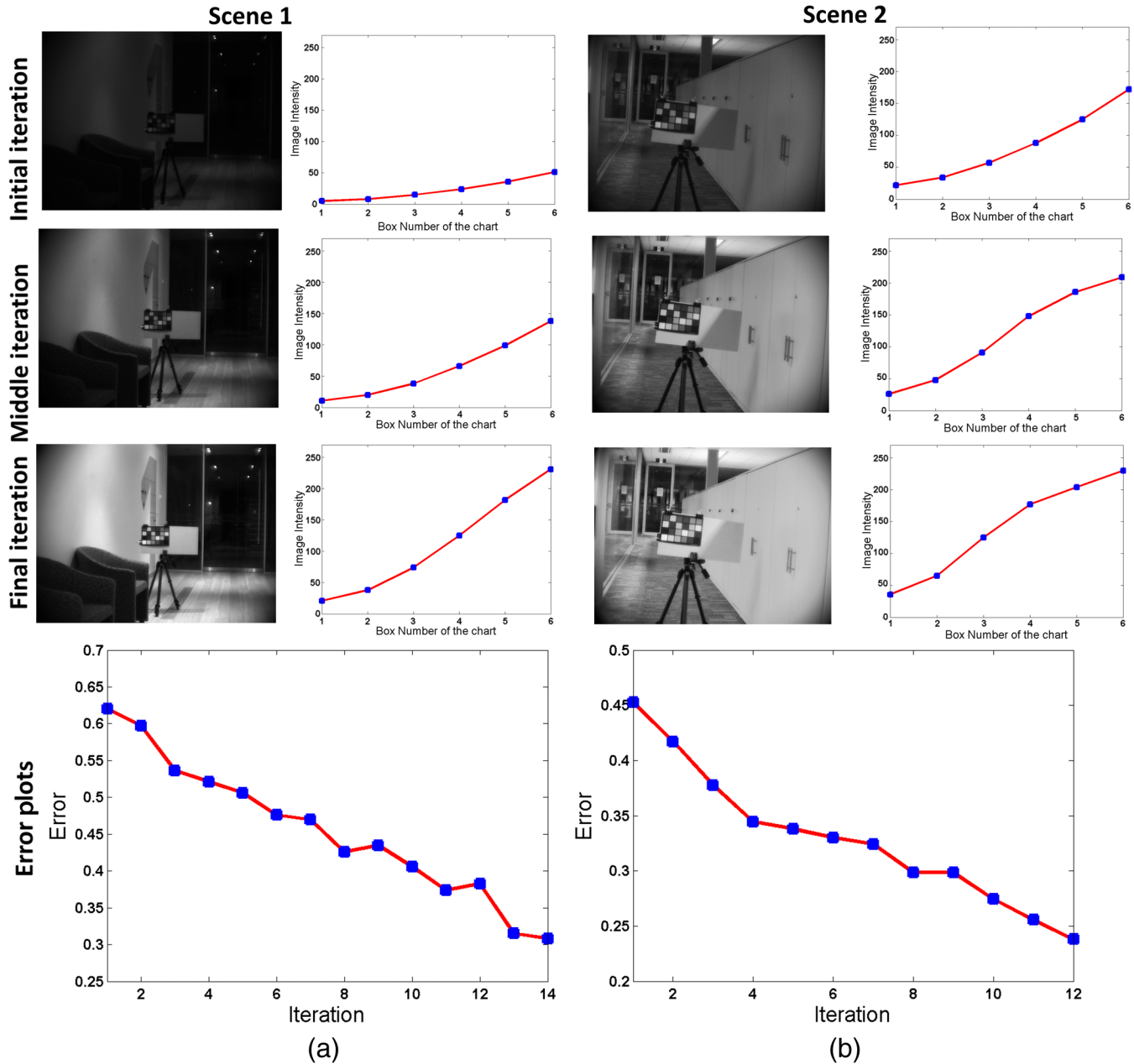


Fig. 2 Opto-knowledge systems, incorporation (OKSI) hyperspectral camera scenes. (a) Spectral power image and (b) color chart gray-tile intensities (the x-axis corresponds to the index of the tile and the y-axis to the photopic response). In this figure, the top row shows the initial images, whereas the second row corresponds to the images produced by the exposure times at the iteration corresponding to the middle point over the convergence of our method. The third row shows the image acquired using the exposure time yielded by our method after convergence has been reached. Finally, the bottom row shows the normalized error plots as a function of iteration number.

We have tested our method using two different imagers. The first of these is a FluxData 3CCD multispectral camera. The second imager is based upon a liquid crystal tunable filter and a QImaging Retiga camera. This system acquires 33 bands in the range between 380 and 700 nm in the intervals of 10 nm. Note that these cameras vary significantly in their architecture. This is so because the former is a multispectral imager where multiple channels share the same exposure time, which is determined by each of the three CCDs comprising the camera. The latter is a staring array system where every wavelength channel can be assigned an individual exposure time. For our experiments, we have placed a

Macbeth ColorChecker in all the scenes under study. These color checkers are widely used in professional photography to perform white balancing or color calibration.²⁹ For purposes of exposure time setting, we use the gray-scale tiles at the bottom row of the chart, which contain six gray-scale colors. These vary from white to black in regular intensity intervals. A well contrasted image can be acquired by setting the exposure such that the photopic response with respect to these gray-scale tiles is linear while maximizing the dynamic range of the camera. In all our experiments, we have set the initial exposure times to 50 ms, threshold to 0.3, and the update step size $\alpha = 0.1$.

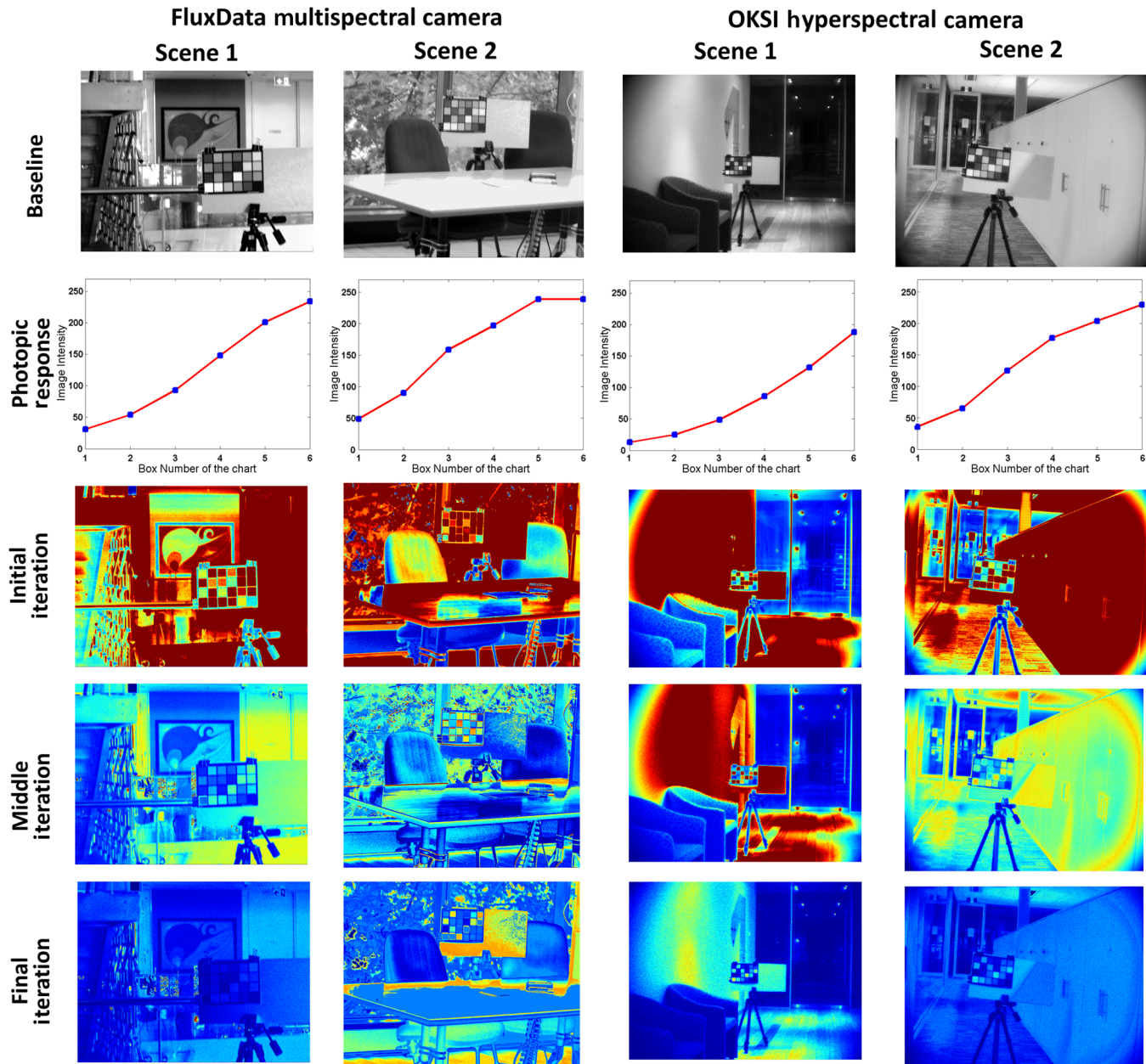


Fig. 3 Baseline images acquired by setting exposure times manually with their photopic response of gray tiles, and per pixel error map of our method at different iterations. From top-to-bottom: baseline image, plot of photopic response of gray tiles in the baseline image, per pixel error map of images at initial, middle, and end iterations of our method. Left-hand columns: scenes acquired by the FluxData multispectral camera; right-hand columns: scenes captured using the OKSI hyperspectral camera. All the error maps are normalized such that blue corresponds to zero and red to unity.

In Fig. 1, we show the results yielded by our method when acquiring two scenes using the FluxData camera. For each scene, we show the spectral power image $\hat{I} = \mathbf{X}T$ of the scene at the initial, middle, and final iterations of our method. Next to each spectral power image, we show its photopic response plot for the gray-scale tiles of the Macbeth ColorChecker. In the plot, the x -axis represents the index of gray-scale tiles, i.e., from black to white, indexed 1 to 6. The y -axis represents the photopic response. At the bottom of each scene, we show the normalized error as a function of iteration number.

From the figure, we can note that the initial spectral power images are noticeably underexposed and, as our method converges, they gradually improve. This is also captured by their photopic response function values as plotted in the figure. Further, as our method iterates to convergence and the contrast of the spectral power image improves with a photopic response over the gray tiles on the color chart approximating a linear response over the whole dynamic range of the camera. Also, from the error plots, we can observe that the method starts with a high error value which gradually decreases toward the threshold.

In Fig. 2, we repeat this sequence for two real-world scenes acquired using the LCTF-based imager. Consistent with our results shown in Fig. 1, our method steadily converges toward the threshold error departing from a typically high value. Also, note that the images delivered at the output depict a much improved contrast as compared to those taken with the initial exposure times. Moreover, the exposure times delivered by our method are almost linear over the dynamic range of the CCDs in the camera.

In Fig. 3, we show in the first column the baseline images acquired by manually setting the exposure times such that the photopic response over the gray tiles (shown in second column) approximates a linear function over the whole dynamic range of the camera. Note that in some cases, the scene lighting conditions in conjunction with the camera setup do not permit the plots to be completely linear. As a result, our baseline images were manually exposed so as to obtain the best linear relationship between the gray tile brightness and the CCD dynamic range. In Fig. 3, we show the absolute error pixel map of our method at the beginning, middle, and end of the iterative process in Algorithm 1. The first two columns correspond to the scenes acquired by the FluxData multispectral camera as shown in Fig. 1. The last two columns correspond to the two scenes acquired by the OKSI hyperspectral camera shown in Fig. 2. From the figure, it can be observed that the error per pixel also reduces as the method iterates.

6 Conclusion

In this paper, we have presented a method for the automatic computation of the exposure times for hyperspectral and multispectral cameras. Here, we have shown how the exposure time can be recovered by using a regularized non-negative least squares optimization. We have also presented a controllability and stability analysis using the state-space representation of our method and illustrated the applicability of our approach for purposes of automatic exposure control of staring array and multi-CCD imaging spectroscopy cameras.

Acknowledgments

NICTA was funded by the Australian Government as represented by the Department of Broadband, Communications, and the Digital Economy and the Australian Research Council through the ICT Centre of Excellence Program.

References

1. L. M. Dale et al., "Hyperspectral imaging applications in agriculture and agro-food product quality and safety control: a review," *Appl. Spectrosc. Rev.* **48**(2), 142–159 (2013).
2. H. Akbari et al., "Cancer detection using infrared hyperspectral imaging," *Cancer Sci.* **102**(4), 852–857 (2011).
3. S. I. Kulasekara et al., "Detection of changes in retinal vessel blood oxygen saturation using hyperspectral imaging," *Invest. Ophthalmol. Visual Sci.* **55**(13), 199 (2014).
4. T. Caras and A. Karnieli, "Ground-level classification of a coral reef using a hyperspectral camera," *Remote Sens.* **7**(6), 7521–7544 (2015).
5. C. Garrido-Novell et al., "Grading and color evolution of apples using RGB and hyperspectral imaging vision cameras," *J. Food Eng.* **113**(2), 281–288 (2012).
6. Z. Khan, A. Mian, and Y. Hu, "Contour code: robust and efficient multi-spectral palmprint encoding for human recognition," in *IEEE Int. Conf. on Computer Vision (ICCV)*, pp. 1935–1942, IEEE (2011).
7. J. Long and S. Li, "Near infrared face image quality assessment system of video sequences," in *Sixth Int. Conf. on Image and Graphics (ICIG)*, pp. 275–279, IEEE (2011).
8. Y. Zhao and N. Liu, "Tensor bidirectional reflectance distribution function model graph based multi-spectral face recognition," in *3rd Int. Congress on Image and Signal Processing (CISP)*, Vol. 4, pp. 1956–1960, IEEE (2010).
9. B. A. Wandell, "The synthesis and analysis of color images," *IEEE Trans. Pattern Anal. Mach. Intell.* **PAMI-9**(1), 2–13 (1987).
10. Y. Schechner, S. Nayar, and P. N. Belhumeur, "A theory of multiplexed illumination," in *Int. Conf. on Computer Vision*, Vol. II, pp. 808–816 (2003).
11. C. Chi, H. Yoo, and M. Ben-Ezra, "Multi-spectral imaging by optimized wide band illumination," *Int. J. Comp. Vision* **86**, 140–151 (2010).
12. M. Trierscheid et al., "Hyperspectral imaging or victim detection with rescue robots," in *IEEE Int. Workshop on Safety, Security and Rescue Robotics*, pp. 7–12, IEEE (2008).
13. D. W. Norwood, "Exposure meter," U.S. Patent No. 2,214,283 (1940).
14. N. R. Nelson, "Light metering means for cameras," U.S. Patent No. 3,282,178 (1966).
15. T. Kuno, H. Sugiura, and N. Matoba, "A new automatic exposure system for digital still cameras," *IEEE Trans. Consum. Electron.* **44**(1), 192–199 (1998).
16. J. Liang, Y. Qin, and Z. Hong, "An auto-exposure algorithm for detecting high contrast lighting conditions," in *7th Int. Conf. on ASIC, 2007 (ASICON'07)*, pp. 725–728, IEEE (2007).
17. C. S. Bell et al., "Determining a final exposure setting automatically for a solid state camera without a separate light metering circuit," U.S. Patent No. US6486915 (2002).
18. S. Shimizu et al., "A new algorithm for exposure control based on fuzzy logic for video cameras," *IEEE Trans. Consum. Electron.* **38**, 617–623 (1992).
19. J.-S. Lee et al., "An advanced video camera system with robust AF, AE, and AWB control," *IEEE Trans. Consum. Electron.* **47**(3), 694–699 (2001).
20. N. Nourani-Vatani and J. Roberts, "Automatic camera exposure control," in *Proc. of the Australasian Conf. on Robotics and Automation* (2007).
21. T. E. Rogers and J. M. Cope, "System and method for camera metering based on flesh tone detection," U.S. Patent No. US7847830 B2 (2010).
22. G. J. Brelstaff et al., "Hyperspectral camera system: acquisition and analysis," *Proc. SPIE* **2587**, 150–159 (1995).
23. A. Sohaib, N. Habili, and A. Robles-Kelly, "Automatic exposure control for multispectral cameras," in *2013 20th IEEE Int. Conf. on Image Processing (ICIP)*, pp. 2043–2047, IEEE (2013).
24. W. Stiles and J. Burch, "Interim report to the commission internationale de l'éclairage zurich 1955, on the national physical laboratory's investigation of colour-matching," *Opt. Acta* **2**, 168–181 (1955).
25. K. B. Burton, C. Owsley, and M. E. Sloane, "Aging and neural spatial contrast sensitivity: photopic vision," *Vision Res.* **33**(7), 939–946 (1993).
26. O. Katsuhiko, *Modern Control Engineering*, Prentice-Hall, Englewood Cliffs, New Jersey (1970).
27. P. B. Stark and R. L. Parker, "Bounded-variable least-squares: an algorithm and applications," *Comput. Stat.* **10**, 129 (1995).
28. N. Bassiou and C. Kotropoulos, "Color image histogram equalization by absolute discounting back-off," *Comp. Vision Image Understand.* **107**(1), 108–122 (2007).
29. C. S. McCamy, H. Marcus, and J. G. Davidson, "A color rendition charts," *J. Appl. Photogr. Eng.* **2**(3), 95–99 (1976).

Ahmed Sohaib received his BS degree in computer system engineering from Ghulam Ishaq Khan Institute of Engineering Sciences and Technology, Pakistan, in 2009. He did graduate course work at National University of Singapore. He is currently working toward his PhD at the Australian National University and National ICT Australia (NICTA). His research interests are toward improving acquisition techniques of imaging systems, with special interest in multispectral and hyperspectral imagers.

Antonio Robles-Kelly received the BEng degree in electronics and telecommunications in 1998 and the PhD degree in computer science from the University of York, United Kingdom, in 2003. Currently, he is a principal researcher and research leader at NICTA and an adjunct associate professor at the ANU. He is also an associate editor of the *IET Computer Vision* and *Pattern Recognition* journals. His research interests are computer vision, statistical pattern recognition, and image processing.